



## A clinical decision support system for predicting cirrhosis stages via high frequency ultrasound images

Xiang Liu<sup>a</sup>, Rui Lin Ma<sup>a</sup>, Jingwen Zhao<sup>a,\*</sup>, Jia Ling Song<sup>b</sup>, Jian Quan Zhang<sup>b</sup>, Shuo Hong Wang<sup>c</sup>

<sup>a</sup> School of Electronic and Electric Engineering, Shanghai University of Engineering Science, Shanghai, China

<sup>b</sup> Department of ultrasound, Changzheng Hospital Affiliated to Second Military Medical University, Shanghai, China

<sup>c</sup> Department of Molecular and Cellular Biology and Center for Brain Science, Harvard University, Cambridge, MA 02138, USA



### ARTICLE INFO

**Keywords:**

Automatic diagnosis  
Liver capsule  
Data split and aggregation scheme  
Capsule-specific CIFAR  
Parenchyma-aimed ResNet  
Cirrhosis

### ABSTRACT

Many visceral organs contain two important structures: capsule and parenchyma. As a non-invasive examination method, ultrasound is widely used. In this study, we develop a computational framework that consists of capsule localization and parenchyma assessment for disease diagnosis.

Clinical decision support system helps providing standard, objective and timely diagnosis. However, although current cirrhosis diagnosis methods are mainly based on the images produced from medical imaging technique and experienced clinicians subjective analysis, many imaging techniques are invasive, and experienced clinicians are in short supply, especially in underdeveloped regions. The proposed system employs an incremental classification model for grading parenchyma patch stages in predicting cirrhosis stages from high frequency ultrasound images. The incremental classification model is based on auto-extracted membrane structures along with patch-ensemble model, using a severe-first strategy. The framework firstly applies multi-scale capsule extraction automatically. The lesions of the capsule and parenchyma show increasing changes in the first three stages. In the final stage, due to the liver ascites, partial lesions restore to normal. To handle the inconsecutive change, the proposed patch-ensemble model applies two layers. We firstly recognize images belong to the severe stage via capsule-specific CIFAR in the first layer. Parenchyma-aimed Resnet is then applied to classify rest images into rest stages. In each layer a data split and aggregation scheme is proposed to evaluate the cirrhosis stage for liver images.

The experimental results demonstrate that the proposed method achieves high precision and effectiveness and can be effectively applied to the auxiliary diagnosis of cirrhosis. Some integral parts of the system are also available for visceral organs with similar structure.

### 1. Introduction

Cirrhosis is a condition in which the liver does not function properly due to long-term damage. This damage is characterized by the replacement of normal liver tissue by scar tissue. In most cases, cirrhosis is a dynamic process of inflammation, hepatocyte damage, necrosis, fibrosis, and regeneration. These changes lead to the conversion of large nodular cirrhosis and small nodular cirrhosis. According to WHO's 2016 statistics (Abubakar et al., 2015), there are about 240 million chronic hepatitis B patients worldwide, and more than 686,000 people die each year from diseases such as cirrhosis and liver cancer. Cirrhosis staging is

proposed to timely discover the course of cirrhosis and take measures to improve the long-term survival rate and quality of life of patients. Especially, for patients with mild cirrhosis, there is no obvious discomfort, and in undeveloped areas medical resources are limited. It results in that many people are not diagnosed until severe cirrhosis. Therefore, investigating the method for screening large-scale populations of cirrhosis is of significance.

As the importance of cirrhosis staging is emphasized, many researchers propose various algorithms (Raeth et al., 1985; Kadah et al., 1996; Krag et al., 2010; McPhee et al., 2010; Wardeh et al., 2011; Mamone et al., 2018). Shimizu et al. (2016) compare serological data

\* Corresponding author.

E-mail addresses: [xliu@sues.edu.cn](mailto:xliu@sues.edu.cn) (X. Liu), [725042549@163.com](mailto:725042549@163.com) (R.L. Ma), [jingwen\\_echo@outlook.com](mailto:jingwen_echo@outlook.com) (J. Zhao), [jialin19810818@126.com](mailto:jialin19810818@126.com) (J.L. Song), [Wintersnow9090@sina.com](mailto:Wintersnow9090@sina.com) (J.Q. Zhang), [wangsh@fas.harvard.edu](mailto:wangsh@fas.harvard.edu) (S.H. Wang).

including  $\sigma$ -GTP and hyaluronic acid, risk factors and serological markers of cirrhosis with the Fontan cycle were evaluated. Smith et al. (2016) determine a computer-based quantitative method to measure liver surface nodules (LSN) in computed tomography (CT) images, as a biomarker for the detection and evaluation of cirrhosis. Qi et al. (2017) collect CT and/or magnetic resonance (MRI) scan images of 105 patients with cirrhosis, the prevalence and clinical features of spontaneous spleno-renal shunt in cirrhosis were assessed. Mamone et al. (2018) analyze the manifestations of liver morphological abnormalities in CT and MRI images in cirrhosis and other diseases, describe the pathological conditions that mimic cirrhosis and help radiologists diagnose cirrhosis and other early diseases. The above methods mainly use serological examination, CT and MRI methods to evaluate the value of assisted diagnosis of cirrhosis. However, serological examination is an invasive examination, and its indicators are more suitable for the dynamic observation of clinical conditions. Techniques such as CT and MRI have a high diagnostic value for space-occupying lesions. Further research is needed for the diagnosis of diffuse diseases such as cirrhosis, and CT and MRI are not suitable for screening large-scale populations of cirrhosis.

Conversely, ultrasound image examination is non-invasive, convenient, reproducible, non-radiative and inexpensive (Planas et al., 2006; Goyal et al., 2009). It is one of the widely used methods of liver examination (Yamaguchi et al., 2002). Ultrasound scan images represent different texture types to reflect the acoustic characteristics of liver tissue (Lelio et al., 1989). In ultrasound image of normal liver, the parenchyma appears as a uniform and uniform distribution of small spots, and the liver capsule appears as a continuous, smooth line-like structure, as shown in Fig. 1(a). In the ultrasound scan of cirrhosis, pseudolobules caused by fibrosis can be seen in the liver parenchyma. The liver capsule appears to be thick or uneven, and ascites appear in the decompensated phase, as shown in Fig. 1(b), the staging of cirrhosis can be achieved using the envelope and substantial above course characteristics.

Based on this, Lee (2013) combines the texture features of M-Band wavelet transform and Gabor wavelet extraction to obtain the texture features of liver parenchyma, but this texture feature could not directly correspond to nodular fibrosis of liver parenchyma. Virmani et al. (2013) use 2D-Gabor wavelet to extract features of liver parenchyma and used SVM to classify it into normal or cirrhosis. Lei et al. (2017) apply fusion of T-LBPs, two-dimensional Gabor transform and K-SVD based dictionary learning methods in cirrhosis recognition of ultrasound (US) images. However, these texture features two literatures applied are inconsistent with the doctor's visual judgment of streak lesions. Liu et al. (2017) use CNN and migration learning to block the tissue characteristics near the envelope line and claim good performance in the second classification problem of "whether it is cirrhosis", providing early screening for cirrhosis. Zhao et al. (2018) extract the geometric features

according to the morphological changes of the liver capsule during cirrhosis, and send them to the support vector machine classifier for multi-level classification, which improves the auxiliary diagnosis accuracy, but the staging effect could not meet the high-precision auxiliary diagnosis requirements. Wang et al. (2016) combine the characteristics of the capsule and the parenchyma with the SVM classifier to grade the degree of cirrhosis. However, this method is sensitive to subtle changes in ultrasound images and is easy to confuse mild and moderate cirrhosis.

Meanwhile, technology-based tools have considerable potential to reduce mortality caused by cirrhosis. Clinical decision support system utilized in the early diagnosis of cirrhosis may allow for the selection of patients at the earliest possible stage of disease development and enable clinicians to initiate the treatment as early in the disease process as possible to more effectively arrest or slow disease progression (Bucholc et al., 2019). To serve as assistant for curing diseases, lots of applications have been developed (Shortliffe and Buchanan, 1975; Lindquist et al., 2008; Afdhal, 2012; Polese, 2014; Morawski et al., 2017). But certain tools focusing on cirrhosis are rare.

In order to overcome these limitations, this paper provides intelligent assistant diagnosis using an incremental classification model, as Fig. 2 shows. The framework aims at grading parenchyma patch stages and predicting cirrhosis stages from high frequency ultrasound images. The proposed incremental classification model is based on auto-extracted capsule along with patch-ensemble model, using a severe-first strategy. Inside the decision support system, the capsule localization part helps doctors labeling membrane-like structures; characteristic extraction of capsule and its adjacent tissue part assists in characterizing the capsule and surrounding tissues; feature extraction and learning of parenchyma part automatically localize lesions in parenchyma. In addition to cirrhosis, other diseases of other organs can also employ these parts.

The main contributions of this paper are summarized as follows:

- Develop clinical decision support system for predicting cirrhosis stages.
- Propose an incremental classification model based on a severe-first strategy. (The first layer recognizes images belonging to the severe stage and the next layer classify rest images into normal, mild and moderate stages.)
- In each layer a data split and aggregation scheme is proposed to evaluate the cirrhosis stage for liver images. Small patches are obtained via a sliding window and patches' votes are then aggregated to classify the candidate image.
- Propose a capsule-specific CIFAR network based on the original CIFAR model to classify individual patches into severe or non-severe stages.

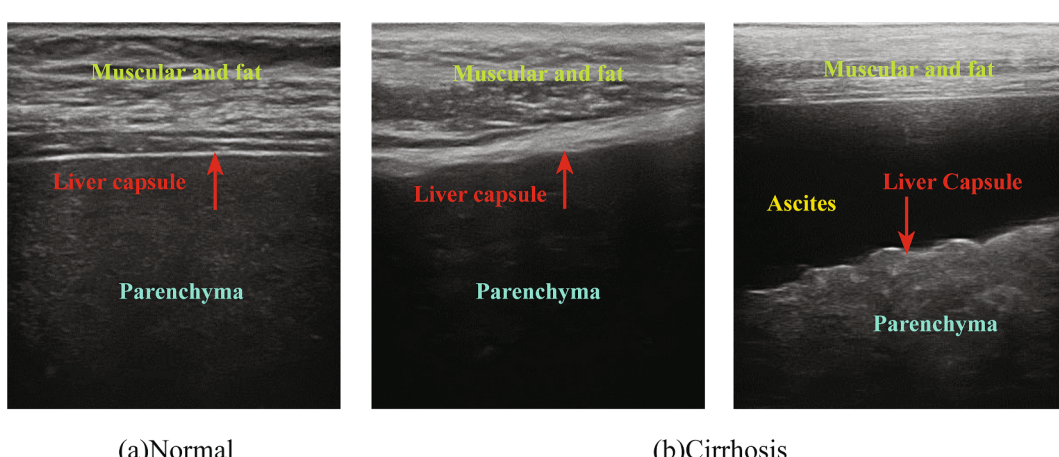


**Fig. 1.** Normal/cirrhosis liver capsules in high frequency ultrasound images.

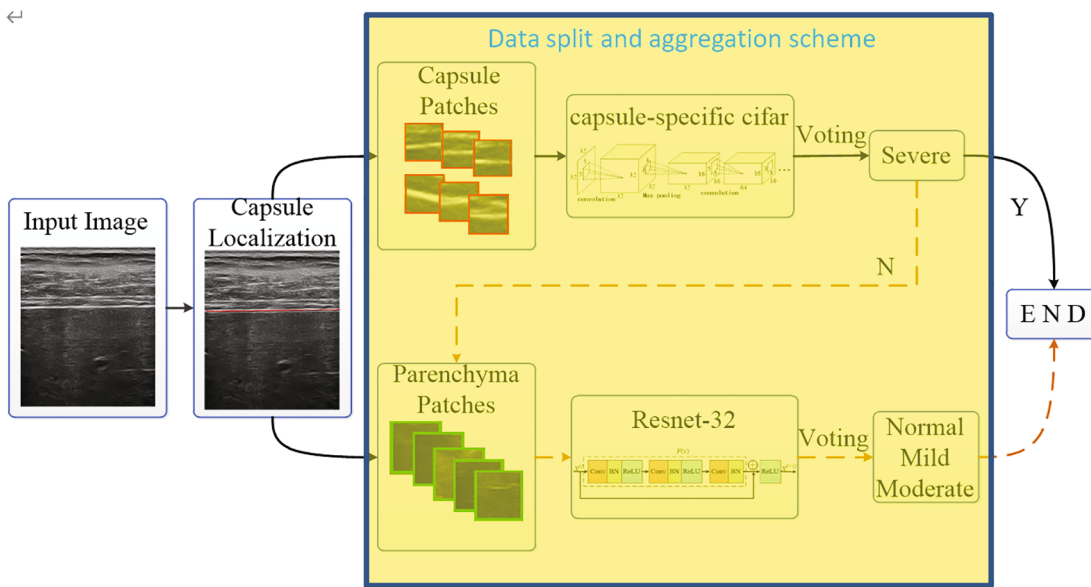


**Fig. 2.** Flowchart of the proposed method.

Experiment results show that, the problem of extracting seriously broken capsule is solved, and the classification accuracy is significantly improved, especially, in the normal stage and severe period.

## 2. Materials and method

### 2.1. Development of a computational framework

#### 2.1.1. Materials

The studies conducted in this paper is provided by the Biomedical Research Ethics Committee of Shanghai Changzheng Hospital (Approval file number: 2017SL013) and all the participants have agreed to participate in the study and signed the informed consent after listening the explanation of the purpose, nature and possible risks of the project.

The surface slice image of liver is obtained by using Volson E8 ultrasonic machine (Model:General Electric (GE) GmbH and Co OG Volson E8, manufacturer: General Electric Medical System Trade Development (China, Shanghai) Limited Company.) whose probe frequency is 4–10 MHZ (Model:Linear Probe 11L-D [4–10 MHz] (BT09+), manufacturer: General Electric Medical System Trade Development (China, Shanghai) Limited Company.). We standardized the ultrasonic examination operation to ensure the acquisition of appropriate images: In the supine or left lateral supine position, the liver tissues were scanned under the xiphoid process and the right intercostal area respectively, the image depth and gain were adjusted to make the liver capsule and superficial liver parenchyma clear, and the two-dimensional high-frequency ultrasound images of the liver capsule in the left and right hepatic lobes were stored respectively. No significant difference was found in age, sex and body weight. Normal and cirrhosis samples were also randomly selected. Liver cirrhosis is divided into 3 stages according to Child-Pugh criteria: mild, moderate and severe. The diagnosis of liver cirrhosis was confirmed by laboratory examination, ultrasonography and CT (Computed Tomography). This article excludes cases of fatty liver, schistosomiasis and other organic liver diseases. The number of employed samples is 68, where the number of normal cases is 20 and the rest belongs to cirrhosis.

Because the size of the body and the thickness of the muscle fat layer are different, ultrasound images of liver tissue in a high resolution is needed by adjusting the distance and frequency of the ultrasonic probe. The height of obtained image is  $262 \pm 36$  and the width is  $375 \pm 29$ .

#### 2.1.2. Capsule localization and incremental classification modeling approach

Liver capsule displays as a bright edge between the upper muscle and fat layer and lower parenchyma in high frequency ultrasound images of liver, due to the different acoustic characteristics of different tissues. Normal liver capsule looks smooth with even thickness. Then with the progression of cirrhosis, the capsule becomes unevenly thickened. In some cases, it even looks as if it's separated into several pieces (Fig. 1).

Based on these morphological observations, we extract image features from liver capsule to help diagnose cirrhosis. Therefore, as the primary step, a robust liver capsule localization method is essential. However, liver capsule is a challenging task, liver ultrasound images from different individuals vary, and image noises widely exist in ultrasound images make the task even harder.

In this paper, we propose an automatic, multi-scale method to accurately localize the liver capsule in liver high frequency ultrasound images. The 'multi-scale' is accomplished by multi-scale filtering. After which regions with varying width similar to liver capsule are enhanced. Then, candidate liver capsules are obtained with a skeleton extraction method. The final liver capsule is determined by solving a multi-object optimization problem.

**2.1.2.1. Multi-scale filtering and skeleton extraction.** The width of liver capsule in different individuals falls in a specific range. Assume all the qualified scales in scale space that may be a liver capsule constitute a set  $S$ . A pixel with scale  $s$  in scale space is denoted as  $(x, y, s)$ . The eigenvalue of Hessian matrix can reflect local image structure feature. The Hessian matrix (denoted as  $H(x, y, s)$ ) at this pixel is calculated by convoluting with second order derivatives of Gaussian at scale  $s$ . Assume  $\lambda_k$  is the  $k$ th largest eigenvalue (absolute value) of Hessian matrix.  $R$  in Eq. 1 reflects the eccentricity of the second order ellipse at  $(x, y)$ ,  $S$  reflects the second order structreness. Pixels on the bright, curved edges in the dark image such as liver capsule have negative  $\lambda_1$ , large  $|R|$  and  $S$ . So, we calculated filtered image  $\rho$  using Eq. 1.

$$\begin{aligned} \rho(x, y) &= \max[\rho(x, y, s)], \quad s \in S \\ \rho(x, y, s) &= \begin{cases} 0, & \lambda_1 > 0 \\ 1 - \exp[-(\alpha R^2 + \beta S^2)], & \text{else} \end{cases} \\ R &= \lambda_1 / |\lambda_2| \\ S &= \sqrt{\lambda_1^2 + \lambda_2^2} \end{aligned} \quad (1)$$

In Fig. 3, Fig. 3(a) is one input liver ultrasound image, Fig. 3(b) is the

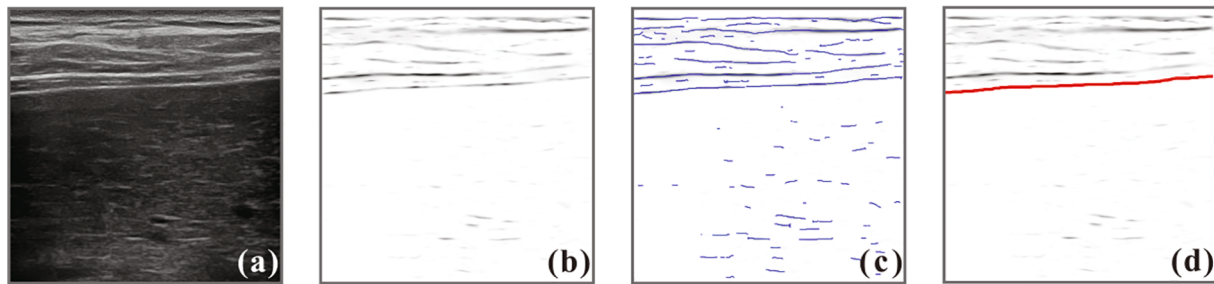


**Fig. 3.** Procedure of liver capsule extraction. (a) Input ultrasound image; (b) Filtered image, the dark curves in it are candidate liver capsules; (c) Candidate liver capsules after skeleton extraction; (d) The obtained liver capsule.

filtered image using Eq. 1.

Then, performing skeleton extraction based on filtered image  $\rho(x,y)$ , we can obtain candidate liver capsules. The candidate capsules are composed of a set of curve segments, written as:  $\Gamma_0 = \{C_i | i = 1, \dots, n_{\Gamma_0}\}$ . Each curve segment  $C_i$  consists of  $n_{C_i}$  discrete points,  $C_i = \{p_{C_i}^j | j = 1, \dots, n_{C_i}\}, p_{C_i}^j = (x_{C_i}^j, y_{C_i}^j)$ . Fig. 3(c) shows an example.

**2.1.2.2. Final capsule localization.** The real liver capsules in high frequency ultrasound images have the following characteristics: 1. Liver capsule is the longest curve in candidate capsule set  $\Gamma_0$  which separates the upper muscle and fat layer and lower parenchyma region. 2. The other candidate curves similar to a real capsule are all above it. To accurately choose right liver capsule from candidate capsules, we proposed a multi-object optimization based method. The final capsule is chosen by solving the following multi-object optimization problem.

$$\begin{aligned} \tau = \operatorname{argmax}_{\Lambda} & \sum_{i=1}^{n_{\Gamma_0}} \Lambda(C_i) [l_{C_i} \cdot \delta(l_{C_i}), \frac{1}{n_{C_i} \cdot n_{\Gamma_0}} \sum_{j=1}^{n_{C_i}} y_i^j] \\ \text{s.t. } & \left\{ \begin{array}{l} \Lambda(x) = \{0, 1\} \\ \bigcap (X_i, X_j) = \emptyset, (i \neq j) \\ \delta(x) = \begin{cases} 0, & x < \varepsilon_l \\ 1, & \text{else} \end{cases} \\ n_{\Gamma} = \sum_{i=1}^{n_{\Gamma_0}} \Lambda(C_i). \end{array} \right. \end{aligned}$$

among which  $l_{C_i}$  denotes the total length of curve segment  $C_i$ ,  $X_i$  represents the  $x$  coordinate set of each final capsule curve segment  $C_i$  in  $\Gamma = \{C_i | i = 1, \dots, n_{\Gamma}\}$ ,  $\Lambda(C_i) = 1$  means  $C_i$  is part of the final capsule segment set. The extracted final liver capsule of Fig. 3(a) is Fig. 3(d). For detailed analysis please see Wang et al. (2016), Frangi et al. (1998).

### 2.1.3. Stage evaluation

After liver capsule is localized, a classification model is needed.

We adopt an incremental model that takes capsule and parenchyma into consideration to classify the cirrhosis stages. The proposed model consists of two layers as illustrated in Fig. 2. Its first layer identifies images of the severe stage and the second layer classifies rest images into rest three stages. Both layers utilize the proposed data split and aggregation scheme.

**2.1.3.1. Data split and aggregation scheme.** Different from images that can be artificially synthesized, collection of ultrasound liver images is limited to the number of patients. Thus the size of dataset is small. However, big data is a prerequisite for classification via learning. If the training data is enough, classification model can be easily trained using deep learning. To overcome the limitation, we adopt a small trick, the

data split and aggregation scheme.

One image is cut into small patches of the same size. There are several advantages. Patches containing imaging noise can be filtered by preprocessing. The vote of patches with better image quality is then aggregated for stage evaluation, which solves the insufficient parameter training.

**2.1.3.2. Data augmentation.** Apparently, the size of liver image dataset provided by the hospital is not enough to support the training of deep network models. The split step of the scheme augments data by splitting images into small patches.

#### A. Training Dataset

The first layer identifies liver images with severe cirrhosis from all samples. However, the data is not balanced (Ripley and Hjort, 1996). Thus, we adopt strategies to augment data (shown in Fig. 4 and Fig. 5, where one strategy is specially designed for the severe stage and strategies for images of capsule and parenchyma are different).

**Capsule:** Assume samples belonging to the severe stage as set  $\Gamma^{CS}$  and the others as set  $\Gamma^{CO}$ . For samples contained in  $\Gamma^{CS}$ , patches are generated by a short sliding window A. These patches are then rotated with small angles to further increase the sample size. Different from the strategy, for images in  $\Gamma^{CO}$  we firstly obtain patches via a long sliding window B before applying the short sliding window A as illustrated in Fig. 4.

**Parenchyma:** Assume samples as set  $\Gamma^{PS}$ . For samples contained in  $\Gamma^{PS}$ , patches are generated by a sliding window C in Fig. 5). These patches are then rotated with small angles to further increase the sample size.

Here, patches are filtered by deleting those whose contrast of Gray-level co-occurrence matrix is no greater than 0.005. The deleted patches belong to background in a relatively high probability.

The starting point, size and step of each window for images at different stages are distinct shown in Table 1.

#### B. Testing Dataset

Test data is the same as the training data. In the training process of convolutional neural network, the training and testing are synchronized. The augmentation data are randomly divided into 4 (training): 1 (testing).

#### C. Validation Dataset

**Capsule:** Samples are split using the same sliding short windows to obtain patches. Unlike the previous step, sliding short windows start from five pixels of the sample, and each step is 20.

**Parenchyma:** Different from training, for images in  $\Gamma^{PO}$  patches are generated by a sliding windows starting from (20, 20) in the sample, and each step is 30.

The goal is to make sure that the tested patches and the trained ones belong to different data distribution.

**2.1.3.3. Aggregation (vote).** Each patch will contribute an individual class label. These labels may be different. But these patches belong to the same parenchyma with only one class label. Thus, we must set a strategy

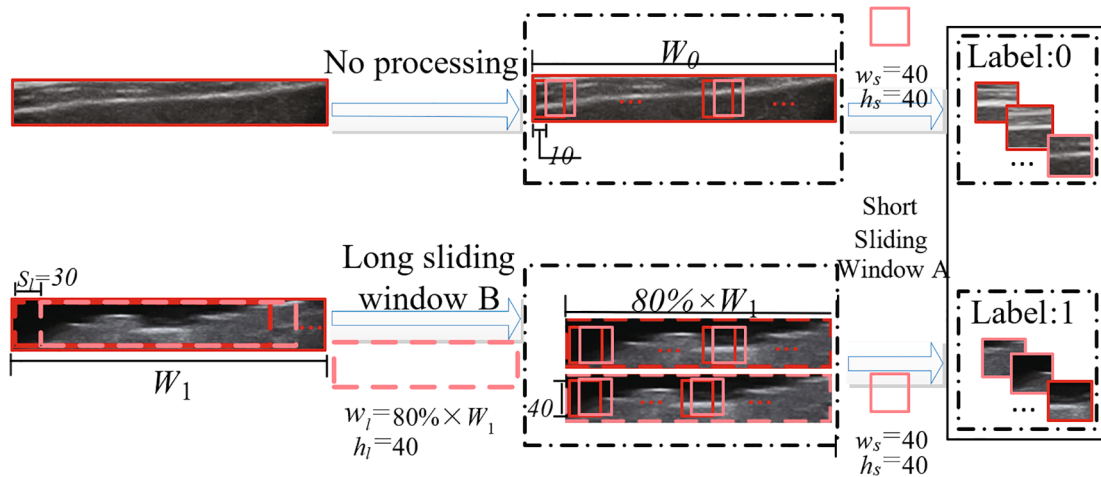


Fig. 4. Capsule augmentation by splitting images into patches.

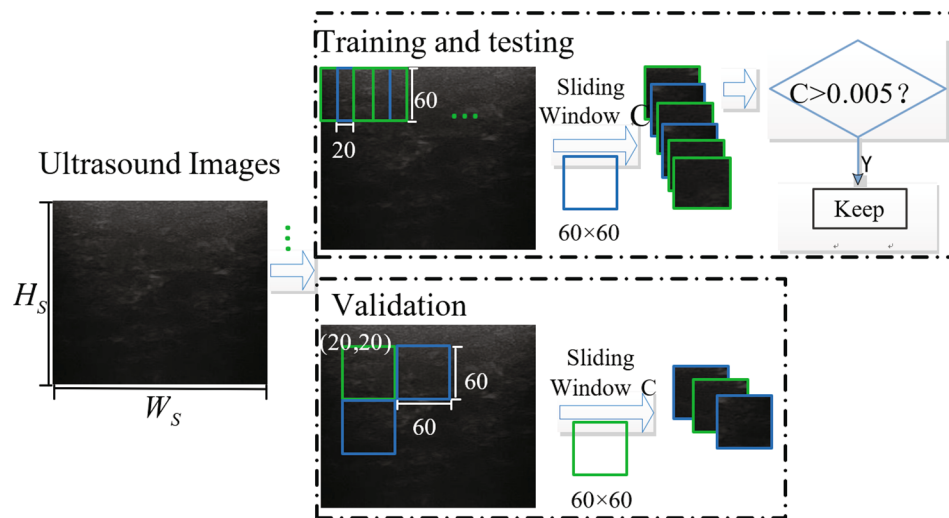


Fig. 5. Parenchyma augmentation by splitting images into patches.

**Table 1**  
Each window for augmentation at different stages are distinct.

|            | Window | Start point (x,y) | Step | Size                   |
|------------|--------|-------------------|------|------------------------|
| Capsule    | A      | (0,0)             | 10   | 40*40                  |
|            | B      | (0,0)             | 10   | 0.8*W <sub>1</sub> *40 |
| Parenchyma | C      | (0,0)             | 10   | 60*60                  |

to aggregate these labels:

$$Score = \frac{\sum_{i=1}^m [l\{Acc_{(Top-1)}^{(i)} \geq \delta\}]}{m} \quad (2)$$

where  $l\{\cdot\}$  is an indicator function,  $Acc_{(Top-1)}$  indicates the Top-1 classification probability. We set  $\delta$  as probability threshold, and finally the  $Score$  for voting is obtained. In order to make the results more convincing, the probability threshold and score are larger than the random number. In the first layer, the probability threshold is 0.7 and Score voting score is 0.6; in the second layer, the probability threshold is 0.6 and Score voting score is 0.5.

**2.1.3.4. Capsule-specific CIFAR.** When the capsule is cut into patches, new problems occur. The capsule may be placed on the upper or lower

side of the patch, the relative position of the capsule and other tissues is not fixed and the small patches are sensitive to noises. Thus it is difficult to train a model. In consideration of convolutional neural network that is famous for feature extraction, we choose CIFAR (Krizhevsky et al., 2009) and make modification to accommodate capsule classification as Fig. 6 shows:

- In order to extract more features, the modified CIFAR add convolution kernels at layer conv-2.
- Apply complex pooling (max for first two layer and average for the last one). Max pooling is good at abstract feature extraction such as texture and average pooling is good at background feature extraction, but we need both.
- To reduce the redundancy of the network and prevent over-fitting, there are less neuron nodes in FC-1 layer.

**2.1.3.5. Parenchyma-aimed Resnet.** As the cirrhosis deteriorate, nodular appear in parenchyma instead of uniform lines and small spots with uniform distribution. We regard the changes as weak features and aggregate parenchyma patches for classification vote. However, traditional classification is usually accompanied by two problems:

1. When extracting high-level semantic features, the classifier is prone to error accumulation and gradient dispersion.

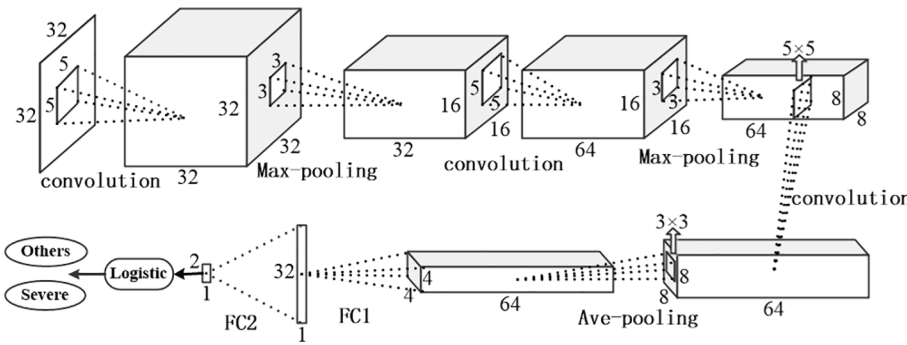


Fig. 6. Architecture of capsule-specific CIFAR.

2. In the mild and moderate stage of cirrhosis, the shape of capsule and the texture of parenchyma has little difference. Thus it is difficult to extract features with high sensitivity for classification.

To solve the questions above, we choose ResNet-32 (He et al., 2016) that consists of multiple sets of residual modules as Fig. 7 illustrates and design the parenchyma-aimed Resnet as Table 2 describes. The size of patch is defined as 60\*60, which is based on the actual texture and the doctor's advice, in order to fully contain the disease course information. Random cropping in patches is to make full use of the information contained, so as to make the trained model more stable. After each patch is cropped, it will be feed into layer conv 1. Such general data pre-processing work can ensure the complete acquisition and full utilization of disease information, and reduce the training parameters. It can be applied to the feature extraction and analysis of organ parenchymal disease.

$$\begin{cases} X^{[l+c]} = f(h(X^{[l]}) + F(x)) \\ F(x) = \sum_{i=l}^{l+c-1} F(x_i) \end{cases} \quad (3)$$

where  $X^{[l]}$  and  $X^{[l+c]}$  are input and output vectors of the residual block respectively.  $F(x)$  denotes the number of convolution layers contained in residual blocks. Each convolution layer is followed by a Batch Normalization(BN) layer (Ioffe and Szegedy, 2015). The BN layer can reduce the scale effect of weights, and the noise caused by normalization has a slight regularization effect. Extracting features by this network can effectively avoid the occurrence of error accumulation or gradient dispersion problems. It is relatively simple to learn identity mapping and extract appropriate features for patches. The structure of the network is shown in Table 2. Finally, three stages of cirrhosis are determined by using the softmax classifier:

$$J(\theta) = -\frac{1}{m} \left[ \sum_{i=1}^m \sum_{j=1}^k |\{y^{(i)} = j\} \log \frac{e^{\theta_j^T x^{(i)}}}{\sum_{l=1}^k e^{\theta_l^T x^{(i)}}} \right] \quad (4)$$

where  $J(\cdot)$  indicates the cost function and minimum classification cross-entropy is obtained via gradient decline algorithms.

## 2.2. Development of clinical decision system

The development of the computational framework introduced above

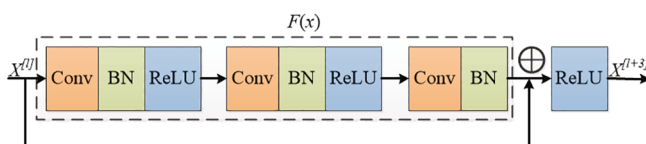


Fig. 7. Architecture of parenchyma-aimed ResNet.

**Table 2**  
The network structure of parenchyma-aimed ResNet.

| Layer name | Output size                   |
|------------|-------------------------------|
| 0          | 32*32                         |
| conv 1     | 32*32                         |
| conv 2     | 32*32                         |
| conv 3     | 16*16                         |
| conv 4     | 8*8                           |
|            | 1*1                           |
|            | random cropping               |
|            | 3*3,16, stride 1              |
|            | [3*3, 16;3*3, 16] * 5         |
|            | [3*3, 32;3*3, 32] * 5         |
|            | [3*3, 64;3*3, 64] * 5         |
|            | Average pool, 3-d fc, softmax |

enables automatically identifying cirrhosis stages. A team of clinical experts and computer scientists was involved in the design process.

To assist the clinicians conveniently, we develop a visual representation system for predicting cirrhosis stages as Fig. 8 shows. After the system is opened, Clinicians chose desired data, and then the predicted results (the clinical stage/level and confidence score) are displayed as suggestion. A single liver slice cannot contain all the information of the liver parenchyma, and cirrhosis is a kind of diffuse lesions which results in that the degree of liver lesions in different sections may not be absolutely the same, and may vary from person to person. Therefore, in order to help the geometrical characteristics of the late analysis, it is required to store at least three section images of different parts. The clinical decision system provides classification results and confidence scores for multiple superficial sections of a patient, so as to facilitate doctors final decision. This further reduces the possibility of misjudgment.

## 3. Experiments and results

### 3.1. Dataset and implementation details

The surface slice image of liver is obtained by using Volson E8 ultrasonic machine with a high frequency. Liver tissue was scanned under xiphoid and between the right ribs. No significant difference was found in age, sex and body weight. Samples were randomly selected, including normal and cirrhosis. The stage of Liver cirrhosis consists mild, moderate and severe on the basis of Child-Pugh criteria. The diagnosis of liver cirrhosis was confirmed by laboratory examination, ultrasonography and CT (Computed Tomography). This article excludes cases of fatty liver, schistosomiasis and other organic liver diseases. The experiment employed 20 normal samples and 48 cirrhosis samples. The different body size and muscle fat layer thickness demand ultrasound images of liver tissue in a high resolution via adjusting the distance and frequency of the ultrasonic probe. That results in the various size of obtained images, whose height is  $262 \pm 36$  and width is  $375 \pm 29$ .

Biomedical Research Ethics Committee of Shanghai Changzheng Hospital is the data provider and all the participants have agreed to participate in the study. Approval file number is 2017SL013.

On account of common network models consume a large number of samples, we extended the samples by sliding window and small angle

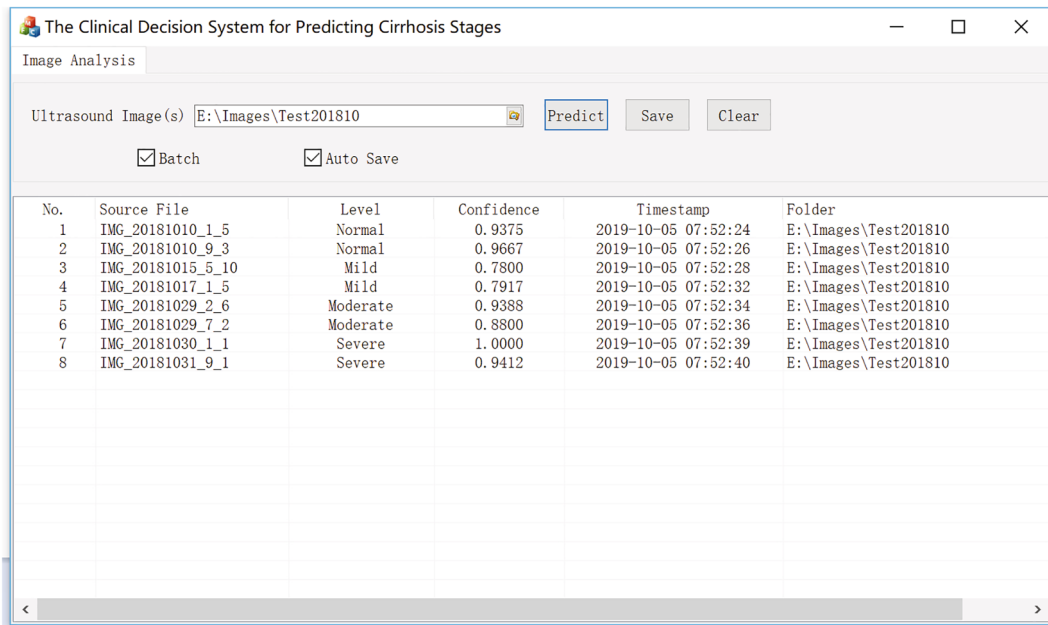


**Fig. 8.** The interface of the an interface of the system.

rotation. During the experiment, there are around 30,000 parenchyma patches and about 120,000 capsule patches after data augmentation.

The experimental environment is as below.

|                     |   |
|---------------------|---|
| CPU                 | AMD Ryzen 2700x 3.7 GHz                         |
| GPU                 | 1080TI*1.                                       |
| Memory              | 16G*2 = 32G DDR4 3000HZ.                        |
| Second level cache  | 4 MB Eight cores and sixteen threads.           |
| Runtime environment | CUDA 8.0, CUDNN 6, OpenCV 2.4.13 and Caffe 1.0. |

Under the environment, the training time of capsule-specific CIFAR is relatively short, 4000 iterations consume about 40 min; while for parenchyma-aimed RestNet training time is longer, 25,000 iterations cost approximately 12 h.

The change of efficiency is tested as Fig. 9. Experiment results demonstrate that the speed doesn't increase much. To distinguish severe cirrhosis, only capsule-specific CIFAR is needed. The network has a shorter time and a higher number of concurrence, but the calculation amount is still stable at a lower level. For the analysis of normal/mild/moderate cirrhosis, parenchyma-aimed RestNet network needs to be added for identification. As the number of concurrent threads increases, the time will increase, but the slope is not high.

### 3.2. Staging of severe cirrhosis

#### 3.2.1. Comparisons among CNN methods

The improved CIFAR network model is used to determine the late stage of liver cirrhosis. The accuracy of network test is 96.30%. The accuracy of CNN network is compared as shown in Fig. 10 and Table 3. The accuracy of CIFAR-B is slightly higher than that of CIFAR-A, which indicates that learning rate has a certain influence on the test results; the accuracy of CIFAR-C is higher than that of CIFAR-B, indicating that the pooling method combination of improved CIFAR network is more suitable for extracting liver capsule features; the accuracy of capsule-specific CIFAR is the highest, which indicates that the improved CIFAR network model performs well in judging the task of severe cirrhosis.

The ROC curve of convolution neural network is shown in Fig. 11. The AUC value of capsule-specific CIFAR is 0.983, which is better than other networks. This shows the ideal classification effect of improved CIFAR network.

#### 3.2.2. Voting method for severe cirrhosis

The confusion matrix (Stehman, 1997) is shown in Table 4 and Table 5 (the percentage of the number determined in parentheses to the

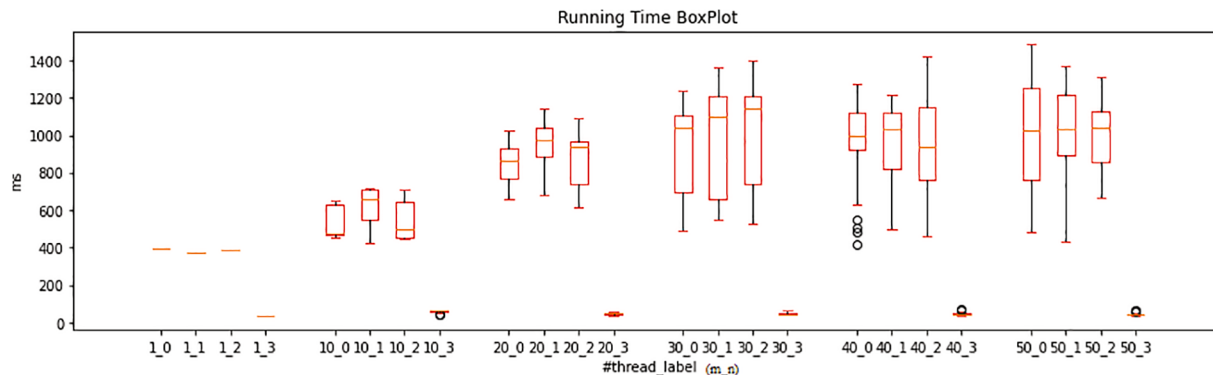


**Fig. 9.** Running time BoxPlot. The thread label on the X-axis is expressed as  $m\_n$ . Letter ' $m$ ' is the number of parallel threads, that is, the number of images of concurrent analysis. The time consumed under 1, 10, 20, 30, 40, and 50 concurrent threads was tested respectively. The letter ' $n$ ' denotes the image of different stages of cirrhosis (0: Normal, 1: mild, 2: moderate, 3: severe).

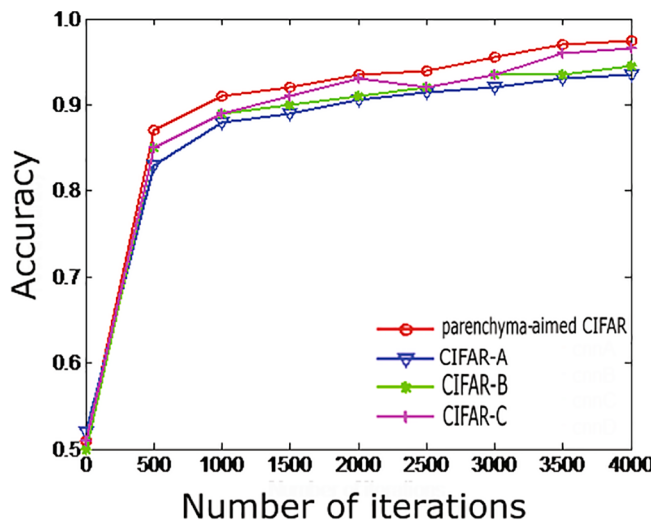


Fig. 10. Comparison curve of CIFAR network accuracy.

**Table 3**  
Comparison test of CIFAR network.

| Network name           | Network Characteristics  | Accuracy (%) |
|------------------------|--|--------------|
| Capsule-specific CIFAR | CIFAR-C + conv-2 number of cnn kernels is 64 + fc-1 output is 32 | 96.30        |
| CIFAR-A                | Original CIFAR Network + 0.0001 learning rate                    | 92.40        |
| CIFAR-B                | Original CIFAR Network + 0.001 learning rate                     | 93.25        |
| CIFAR-C                | CIFAR-B + conv-2 pooling method is max-max-ave                   | 95.10        |

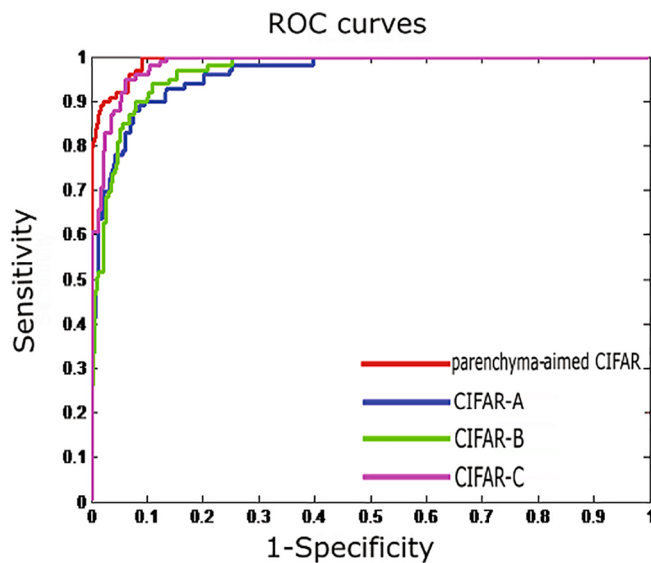


Fig. 11. ROC curve diagram.

**Table 4**  
First-layer network decision result graph (a).

| True stage | Others | Predicted stage |           |
|------------|--------|-----------------|-----------|
|            |        | Others          | Severe    |
|            | Others | 98.2%(54)       | 1.8%(1)   |
|            | Severe | 7.7%(1)         | 92.3%(12) |

**Table 5**  
First-layer network decision result graph (b).

| True stage |          | Predicted stage |          |           |           |
|------------|----------|-----------------|----------|-----------|-----------|
|            |          | Normal          | Mild     | Moderate  | Severe    |
| Normal     | Normal   | 100%(20)        | 0%(0)    | 0%(0)     | 0%(0)     |
| Mild       | Mild     | 0%(0)           | 100%(18) | 0%(0)     | 0%(0)     |
| Moderate   | Moderate | 0%(0)           | 0%(0)    | 94.1%(16) | 5.9%(1)   |
| Severe     | Severe   | 0%(0)           | 0%(0)    | 7.7%(1)   | 92.3%(12) |

total number of samples in this period). The results show that one moderate cirrhosis sample is misclassified as severe cirrhosis, and one severe cirrhosis sample is misclassified as moderate cirrhosis, which demonstrates the accuracy of the proposed method.

### 3.3. Staging of normal, mild and moderate cirrhosis

#### 3.3.1. Comparisons between ResNet network models

In order to verify the experimental results, resnet-20 and resnet-56 are used as comparative experiments. The experimental results are shown in Fig. 7 and Table 6. According to the results of accuracy, resnet-20 is the worst in three classifications of normal, mild and moderate cirrhosis. The accuracy of resnet-32 and resnet-56 is 94.8% and 96.3% respectively after 25,000 iterations. But resnet-56 has deep network, high computational complexity and long training time. Therefore, resnet-32 is chosen to classify normal, mild and moderate cirrhosis.

#### 3.3.2. Determining the remaining three periods

The confusion matrix is shown in Table 7 and Table 8 (the percentage of the number determined in parentheses to the total number of individuals in the period). One normal sample was misclassified as mild cirrhosis, and two mild cirrhosis samples were misclassified as moderate cirrhosis.

### 3.4. Robustness test after synthesizing two-level classification results

Combining with voting method, an improved CIFAR network model based on the characteristics of patch patches in liver capsule misclassifies a moderate cirrhosis sample into severe cirrhosis. ResNet neural network based on patch features of liver parenchyma misclassifies a normal sample into mild cirrhosis and two mild cirrhosis samples into moderate cirrhosis. The results of two-level classification are synthesized and the confusion matrix is obtained as shown in Tables 7 and 8.

We also perform another test: We change the data that will enter the classification network to adjust the acquisition step of capsule and parenchyma patch, for the robustness test. Table 9 shows the stable performance. Since we predict cirrhosis via a patch-to-patches-voting strategy, essentially, we make full use of the disease course information contained in the slice and the results have better fault tolerance.

### 3.5. Comparison with other methods

Compared with other methods, as shown in Table 10, Lee et al. (2003) combined the texture features extracted by M-Band wavelet transform and Gabor wavelet to obtain the texture features of liver parenchyma. Virmani et al. (2013) used 2D-Gabor wavelet to extract features of liver parenchyma, and classified them into normal or cirrhosis

**Table 6**  
Comparisons between ResNet network models.

| Network name | Network type | Accuracy (%) |
|--------------|--------------|--------------|
| cnn-r20      | ResNet-20    | 89.75        |
| cnn-r32      | ResNet-32    | 94.80        |
| cnn-r56      | ResNet-56    | 96.30        |

**Table 7**  
The second-layer result diagram (a).

|            |          | Predicted stage |           |          |
|------------|----------|-----------------|-----------|----------|
|            |          | Normal          | Mild      | Moderate |
| True stage | Normal   | 95%(19)         | 5%(1)     | 0%(0)    |
|            | Mild     | 0%(0)           | 88.9%(16) | 11.1%(2) |
|            | Moderate | 0%(0)           | 0%(0)     | 100%(16) |

**Table 8**  
The second-layer result diagram (b).

|            |          | Predicted stage |           |           |           |
|------------|----------|-----------------|-----------|-----------|-----------|
|            |          | Normal          | Mild      | Moderate  | Severe    |
| True stage | Normal   | 95%(19)         | 5%(1)     | 0%(0)     | 0%(0)     |
|            | Mild     | 0%(0)           | 88.9%(16) | 11.1%(2)  | 0%(0)     |
|            | Moderate | 0%(0)           | 0%(0)     | 94.1%(16) | 5.9%(1)   |
|            | Severe   | 0%(0)           | 0%(0)     | 7.7%(1)   | 92.3%(12) |

**Table 9**  
Step change for robustness test.

| Capsule Step       | Parenchyma Step | Accuracy |       |          |        |
|--------------------|-----------------|----------|-------|----------|--------|
|                    |                 | Normal   | Mild  | Moderate | Severe |
| 20                 | 30              | 0.950    | 0.889 | 0.941    | 0.923  |
| 15                 | 25              | 1.000    | 0.889 | 0.941    | 1.000  |
| 18                 | 22              | 1.000    | 0.944 | 0.941    | 0.846  |
| 22                 | 38              | 1.000    | 0.833 | 0.941    | 0.923  |
| 25                 | 35              | 1.000    | 0.833 | 0.941    | 1.000  |
| Mean               |                 | 0.990    | 0.878 | 0.941    | 0.938  |
| Standard deviation |                 | 0.022    | 0.046 | 0.000    | 0.064  |

**Table 10**  
Accuracy comparisons with the state-of-the-art methods.

| Methods               | Normal (%)   |              | Cirrhosis    |              |  |
|-----------------------|--------------|--------------|--------------|--------------|--|
|                       | Mild (%)     | Moderate (%) | Severe (%)   |              |  |
| The proposed          | <b>95.00</b> | <b>88.90</b> | <b>94.10</b> | 92.30        |  |
| Zhao et al. (2018)    | 91.36        | 72.45        | 69.83        | 81.14        |  |
| Liu et al. (2017)     | 92.08        | 80.23        | 75.12        | <b>93.58</b> |  |
| Wang et al. (2016)    | 92.46        | 80.49        | 83.93        | 91.98        |  |
| Virmani et al. (2013) | 71.29        | 66.67        | 70.40        | 74.46        |  |
| Lee et al. (2003)     | 68.15        | 67.80        | 67.43        | 70.66        |  |

by support vector machine classifier (SVM). Zhao et al. (2018) extracted geometric features according to the morphological changes of hepatic capsule in the course of cirrhosis and sent them to support vector machine classifier for multi-level classification. Liu et al. (2017) quantitatively analyzed the cirrhosis stage by using geometric features of liver capsule and texture features of liver parenchyma, and extracted the geometric features of liver capsule based on its linear structure. However, relevant information of tissues around the capsule is ignored. The texture features of the liver parenchyma describe the global picture of the parenchyma, whereas cirrhosis is localized and heterogeneous, and the characteristic information may be diluted. Wang et al. (2016) used SVM classifier to classify the degree of liver cirrhosis combined with the characteristics of capsule and substance. The method proposed in this paper is based on the deep neural network model to learn the patch features, and combined with two-level classification and voting method to staging cirrhosis stages. It achieves higher accuracy than other methods except the severe stage. But we were able to achieve roughly the same accuracy just by using the capsule and tissues nearby while other methods utilize both capsule and parenchyma. In this paper, the deep neural network model is used to automatically learn the features of the envelope and the real patch blocks, and the global classification is

realized by combining the two-level classification and voting method. The residual neural network model proposed in this paper can overcome the shortcomings of gradient disappearance in the deep network.

### 3.6. Development of clinical decision support system

The architecture of application-engine in Fig. 12 is proposed in the clinical decision support system. The application is responsible for providing GUI interface which includes obtaining ultrasound image directly from ultrasound imaging equipment, importing ultrasound image by user, and displaying the result, etc. The engine is used as the analysis engine to automatically locate the capsule, segment the capsule, its adjacent tissues and liver parenchyma from the image, and then carry out the cirrhosis classification based on different designed DNN. The application and the engine interact through pipe communication mechanism.

This architecture realizes the separation of application and core algorithm, and has better flexibility. The application can be customized freely according to different requirements and application scenarios. The analysis process of engine is designed with multi-thread, which provides parallel processing capability and the support for large-scale and stacked applications.

The developed system is currently being tested in Luoyang Chinese Medicine Hospital where experienced clinicians of cirrhosis are in need.

## 4. Discussions

To prove the system can be generalized in principle, we conduct experiments on predicting liver fibrosis stages. Fibrosis is more difficult than cirrhosis for the more slighter texture changes of the liver parenchyma in this disease. On the rabbit liver fibrosis data set provided by Shanghai Changzheng Hospital of the Second Military Medical University, the course of liver fibrosis is divided into four stages: S0 denotes normal and no fibrosis; S1 is expanded fibrosis in the portal area; S2 denotes the fibrosis around the portal area with a fibrous septal structure. S3 is a large number of fibrous septa, lobules disorganized, and no hard nodules; S4 represents for early cirrhosis.

Firstly, the image of the liver parenchyma is rotated and cut into small pieces to expand the data set. Considering the small texture changes among the stages of liver fibrosis, ResNet V2 (ResNet enhancement model)(He et al., 2016) is selected. The ImageNet data set is used for pre training and initialization of the weight parameters of each layer. The expanded data set is trained for fine-tuning of various parameters, then the Softmax classifier realizes the four classification of small pieces. Finally, predict stages of fibrosis combined with the voting principle. The sensitivity, specificity and Fscore of liver fibrosis at S0-S4 stage are shown in Table 11.

The experimental results show that the method presented in this paper has good generality for the classification of diffuse tissue lesions. Through discussion with doctors, we agree that the method presented in this paper has good applicability to liver diseases, such as fatty liver and schistosomiasis liver disease, and other diseases, including hyperthyroidism, Hashimoto thyroiditis, and breast adenopathy.

## 5. Conclusions

Clinical decision support system can help to provide standard, objective and timely cirrhosis diagnosis. However, although current cirrhosis diagnosis methods are mainly based on the images produced from medical imaging technique and experienced clinicians subjective analysis, many imaging techniques are invasive, and experienced clinicians are in short supply, especially in underdeveloped regions. In this study, an auxiliary diagnostic system is proposed, which utilizes an incremental classification model for grading parenchyma patch stages in predicting cirrhosis stages from high frequency ultrasound images. The proposed incremental classification model is based on auto-extracted

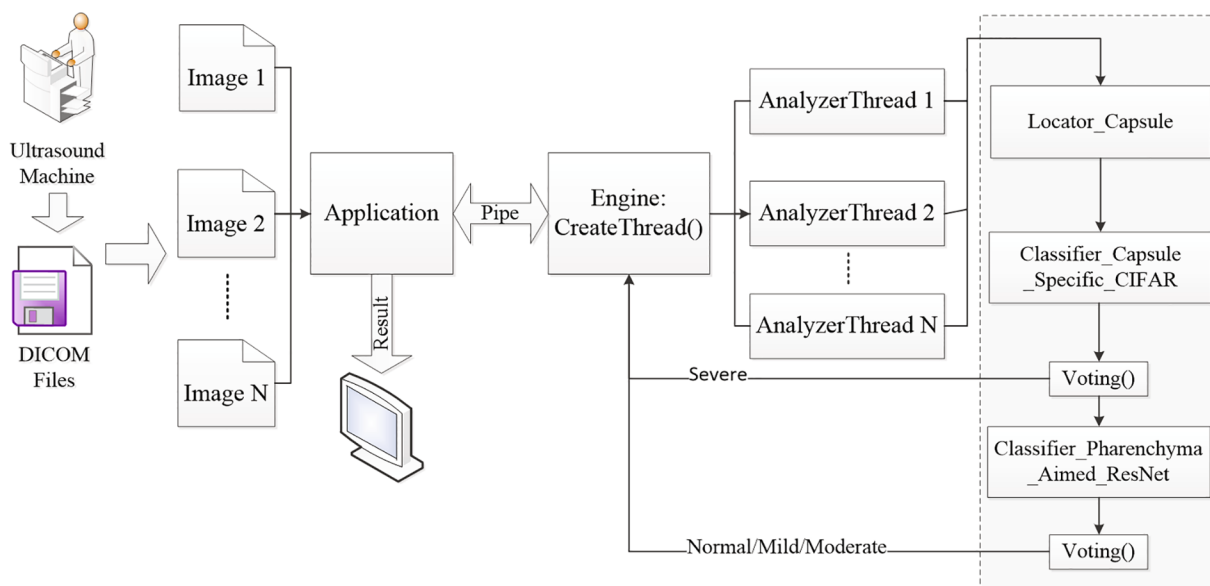


Fig. 12. The architecture of the system.

**Table 11**

Classification results of liver fibrosis stages.

| Metric      | S0–S1 (%) | S2 (%) | S3 (%) | S4 (%) |
|-------------|-----------|--------|--------|--------|
| Sensitivity | 93.75     | 96.88  | 87.50  | 91.30  |
| Specificity | 93.75     | 93.94  | 95.45  | 87.50  |
| F1-score    | 93.75     | 95.39  | 91.30  | 89.36  |

capsule along with patch-ensemble model, using a severe-first strategy.

The proposed approach firstly applies multi-scale liver capsule extraction automatically. The lesions of the liver capsule and liver parenchyma show increasing changes in the first three stages. In the final stage, due to the liver ascites, the changes suddenly changed, and then some lesions restore to normal and new changes occur. To handle the inconsecutive changes, the proposed patch-ensemble model applies two layers to avoid classifying images into four stages in one go. We firstly recognize images belong to the severe stage via capsule-specific CIFAR in the first layer. Parenchyma-aimed Resnet-32 is then applied to classify rest images into rest stages. In each layer a data split and aggregation scheme is proposed to evaluate the cirrhosis stage for liver images.

The experimental results demonstrate that the proposed method achieves high precision and effectiveness and can be effectively applied to the auxiliary diagnosis of cirrhosis. This framework is also applicable to liver diseases such as fibrosis, liver steatosis, schistosomiasis liver disease, and other diseases including hyperthyroidism, Hashimoto's thyroiditis, breast adenopathy, etc.

#### Author contributions

Xiang Liu, Rui Lin Ma and Jing Wen Zhao proposed the idea and wrote the paper. Jia Lin Song, Jian Quan Zhang, Xiang Liu, Rui Lin Ma worked on the data gathering, the images analyzing and the experiments analyzing based on the equipment of high-frequency ultrasound. Xiang Liu, Rui Lin Ma, Jing Wen Zhao and Shuo Hong Wang worked on the algorithm implementation. Jing Wen Zhao supervised the research work.

#### Declaration of Competing Interest

The authors declare that they have no known competing financial interests or personal relationships that could have appeared to influence

the work reported in this paper.

#### Acknowledgements

This work was supported by 1) Science and Technology Commission of Shanghai Municipality: No.19ZR1421500 and 2) Youth National Natural Science Foundation of China: Grant No.81101105. This study was approved by the Biomedical Research Ethics Committee of Shanghai changzheng hospital (Approval file number: 2017SL013). We thank all the participants who have agreed to participate in the study and signed the informed consent after listening the explanation of the purpose, nature and possible risks of the project.

#### References

- Abubakar, I., Tillmann, T., & Banerjee, A. (2015). Global, regional, and national age-sex specific all-cause and cause-specific mortality for 240 causes of death, 1990–2013: A systematic analysis for the global burden of disease study 2013. *Lancet*, *385*, 117–171.
- Afdhal, N. H. (2012). Fibroscan (transient elastography) for the measurement of liver fibrosis. *Gastroenterology & Hepatology*, *8*, 605.
- Bucholc, M., Ding, X., Wang, H., Glass, D. H., Wang, H., Prasad, G., Maguire, L. P., Bjourson, A. J., McClean, P. L., Todd, S., et al. (2019). A practical computerized decision support system for predicting the severity of alzheimer's disease of an individual. *Expert Systems With Applications*, *130*, 157–171.
- Di Lelio, A., Cestari, C., Lomazzi, A., & Beretta, L. (1989). Cirrhosis: Diagnosis with sonographic study of the liver surface. *Radiology*, *172*, 389–392.
- Frangi, A. F., Niessen, W. J., Vincken, K. L. & Viergever, M. A. (1998). Multiscale vessel enhancement filtering. In International conference on medical image computing and computer-assisted intervention (pp. 130–137). Springer.
- Goyal, N., Jain, N., Rachapalli, V., Cochlin, D., & Robinson, M. (2009). Non-invasive evaluation of liver cirrhosis using ultrasound. *Clinical Radiology*, *64*, 1056–1066.
- He, K., Zhang, X., Ren, S., & Sun, J. (2016). Deep residual learning for image recognition. In Proceedings of the IEEE conference on computer vision and pattern recognition (pp. 770–778).
- He, K., Zhang, X., Ren, S. & Sun, J. (2016b). Identity mappings in deep residual networks (pp. 630–645).
- Ioffe, S. & Szegedy, C. (2015). Batch normalization: Accelerating deep network training by reducing internal covariate shift. arXiv preprint arXiv:1502.03167.
- Kadah, Y. M., Farag, A. A., Zurada, J. M., Badawi, A. M., & Youssef, A.-B. (1996). Classification algorithms for quantitative tissue characterization of diffuse liver disease from ultrasound images. *IEEE Transactions on Medical Imaging*, *15*, 466–478.
- Krag, A., Bendtsen, F., Henriksen, J. H., & Møller, S. (2010). Low cardiac output predicts development of hepatorenal syndrome and survival in patients with cirrhosis and ascites. *Gut*, *59*, 105–110.
- Krizhevsky, A., Hinton, G., et al. (2009). Learning multiple layers of features from tiny images. *Technical Report Citeseer*.
- Lee, W.-L. (2013). An ensemble-based data fusion approach for characterizing ultrasonic liver tissue. *Applied Soft Computing*, *13*, 3683–3692.

- Lee, W.-L., Chen, Y.-C., & Hsieh, K.-S. (2003). Ultrasonic liver tissues classification by fractal feature vector based on m-band wavelet transform. *IEEE Transactions on Medical Imaging*, 22, 382–392.
- Lei, Y., Zhao, X., Wang, G., Yu, K., & Guo, W. (2017). A novel approach for cirrhosis recognition via improved lbp algorithm and dictionary learning. *Biomedical Signal Processing and Control*, 38, 281–292.
- Lindquist, A. M., Johansson, P. E., Petersson, G. I., Saveman, B.-I., & Nilsson, G. C. (2008). The use of the personal digital assistant (pda) among personnel and students in health care: A review. *Journal of Medical Internet Research*, 10, Article e31.
- Liu, X., Song, J., Wang, S., Zhao, J., & Chen, Y. (2017). Learning to diagnose cirrhosis with liver capsule guided ultrasound image classification. *Sensors*, 17, 149.
- Liu, X., Zhan, Z., Yan, M., Zhao, J., Song, J., & Chen, Y. Q. (2017). Computer-aided cirrhosis diagnosis via automatic liver capsule extraction and combined geometry-texture features. In *2017 IEEE international conference on multimedia and expo (ICME)* (pp. 865–870). IEEE.
- Mamone, G., Cortis, K., Sarah, A., Caruso, S., & Miraglia, R. (2018). Hepatic morphology abnormalities: Beyond cirrhosis. *Abdominal Radiology*, 43, 1612–1626.
- McPhee, S. J., Papadakis, M. A., Rabow, M. W., et al. (2010). *Current medical diagnosis & treatment 2010*. McGraw-Hill Medical New York.
- Morawski, K., Ghazinouri, R., Krumme, A., McDonough, J., Durfee, E., Oley, L., Mohta, N., Juusola, J., & Choudhry, N. K. (2017). Rationale and design of the medication adherence improvement support app for engagement/blood pressure (medisafe-bp) trial. *American Heart Journal*, 186, 40–47.
- Planas, R., Montoliu, S., Balleste, B., Rivera, M., Miquel, M., Masnou, H., Galeras, J. A., Giménez, M. D., Santos, J., Cirera, I., et al. (2006). Natural history of patients hospitalized for management of cirrhotic ascites. *Clinical Gastroenterology and Hepatology*, 4, 1385–1394.
- Polese, G. (2014). A decision support system for evidence based medicine. *Journal of Visual Languages & Computing*, 25, 858–867.
- Qi, X., Qi, X., Zhang, Y., Shao, X., Wu, C., Wang, Y., Wang, R., Zhang, X., Deng, H., Hou, F., et al. (2017). Prevalence and clinical characteristics of spontaneous splenorenal shunt in liver cirrhosis: A retrospective observational study based on contrast-enhanced computed tomography (ct) and magnetic resonance imaging (mri) scans. *Medical Science Monitor: International Medical Journal of Experimental and Clinical Research*, 23, 2527.
- Raeth, U., Schlaps, D., Limberg, B., Zuna, I., Lorenz, A., Van Kaick, G., Lorenz, W. J., & Kommerell, B. (1985). Diagnostic accuracy of computerized b-scan texture analysis and conventional ultrasonography in diffuse parenchymal and malignant liver disease. *Journal of Clinical Ultrasound*, 13, 87–99.
- Ripley, B. D., & Hjort, N. (1996). *Pattern recognition and neural networks*. Cambridge University Press.
- Shimizu, M., Miyamoto, K., Nishihara, Y., Izumi, G., Sakai, S., Inai, K., Nishikawa, T., & Nakanishi, T. (2016). Risk factors and serological markers of liver cirrhosis after Fontan procedure. *Heart and Vessels*, 31, 1514–1521.
- Shortliffe, E. H., & Buchanan, B. G. (1975). A model of inexact reasoning in medicine. *Mathematical Biosciences*, 23, 0–379.
- Smith, A. D., Branch, C. R., Zand, K., Subramony, C., Zhang, H., Thaggard, K., Hosch, R., Bryan, J., Vasani, A., Griswold, M., et al. (2016). Liver surface nodularity quantification from routine ct images as a biomarker for detection and evaluation of cirrhosis. *Radiology*, 280, 771–781.
- Stehman, S. V. (1997). Selecting and interpreting measures of thematic classification accuracy. *Remote Sensing of Environment*, 62, 77–89.
- Virmani, J., Kumar, V., Kalra, N., & Khandelwal, N. (2013). Prediction of liver cirrhosis based on multiresolution texture descriptors from b-mode ultrasound. *International Journal of Convergence Computing*, 1, 19–37.
- Wang, S. H., Liu, X., Zhao, J., Song, J. L., Zhang, J. Q., & Chen, Y. Q. (2016). Learning to diagnose cirrhosis via combined liver capsule and parenchyma ultrasound image features. In *2016 IEEE international conference on bioinformatics and biomedicine (BIBM)* (pp. 799–804). IEEE.
- Wardeh, R., Lee, J. G., & Gu, M. (2011). Endoscopic ultrasound-guided paracentesis of ascitic fluid: A morphologic study with ultrasonographic correlation. *Cancer Cytopathology*, 119, 27–36.
- Yamaguchi, T., Hachiya, H., Kamiyama, N., & Moriyasu, F. (2002). Examination of the spatial correlation of statistics information in the ultrasonic echo from diseased liver. *Japanese Journal of Applied Physics*, 41, 3585.
- Zhao, J., Wang, S. H., Liu, X., Liu, Y., & Chen, Y. Q. (2018). Early diagnosis of cirrhosis via automatic location and geometric description of liver capsule. *The Visual Computer*, 34, 1677–1689.